

Magnetic reconnection process in transient coaxial helicity injection

F. Ebrahimi, E. B. Hooper, C. R. Sovinec, and R. Raman

Citation: *Phys. Plasmas* **20**, 090702 (2013); doi: 10.1063/1.4821974

View online: <http://dx.doi.org/10.1063/1.4821974>

View Table of Contents: <http://pop.aip.org/resource/1/PHPAEN/v20/i9>

Published by the AIP Publishing LLC.

Additional information on Phys. Plasmas

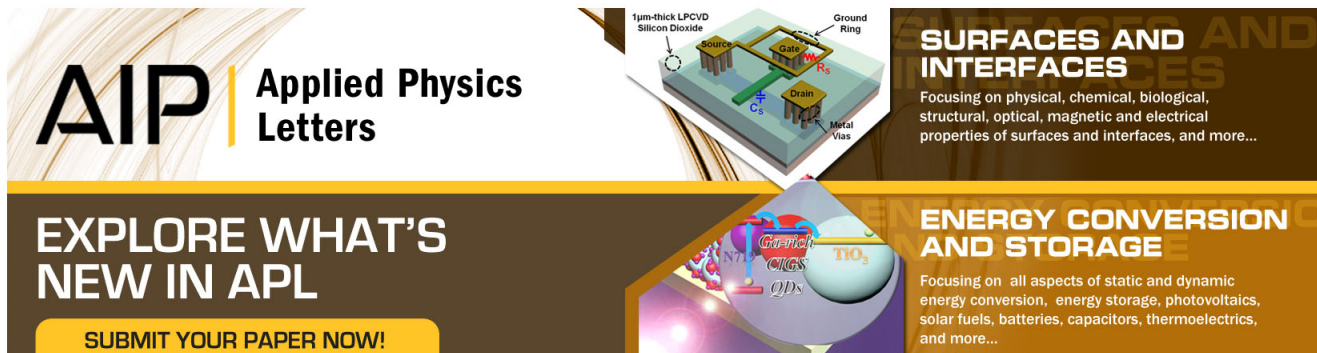
Journal Homepage: <http://pop.aip.org/>

Journal Information: http://pop.aip.org/about/about_the_journal

Top downloads: http://pop.aip.org/features/most_downloaded

Information for Authors: <http://pop.aip.org/authors>

ADVERTISEMENT



AIP | Applied Physics Letters

SURFACES AND INTERFACES
Focusing on physical, chemical, biological, structural, optical, magnetic and electrical properties of surfaces and interfaces, and more...

ENERGY CONVERSION AND STORAGE
Focusing on all aspects of static and dynamic energy conversion, energy storage, photovoltaics, solar fuels, batteries, capacitors, thermoelectrics, and more...

EXPLORE WHAT'S NEW IN APL

SUBMIT YOUR PAPER NOW!

Labels in the 3D schematic: 1µm-thick LPCVD Silicon Dioxide, Source, Drain, Metal Vias, Ground Ring, Gate, C_1 , C_2 , R_1 , R_2 .

Labels in the energy conversion diagram: NO_2 , CO_2 , CH_4 , QDs , NO_3 .

Magnetic reconnection process in transient coaxial helicity injection

F. Ebrahimi,^{1,(a)} E. B. Hooper,² C. R. Sovinec,³ and R. Raman⁴

¹*Department of Astrophysical Sciences, Princeton University, Princeton, New Jersey 08544, USA*

²*Lawrence Livermore National Laboratory, Livermore, California 94550, USA*

³*University of Wisconsin, Madison, Wisconsin 53706, USA*

⁴*University of Washington, Seattle, Washington 98195, USA*

(Received 30 July 2013; accepted 2 September 2013; published online 17 September 2013)

The physics of magnetic reconnection and fast flux closure in transient coaxial helicity injection experiments in NSTX is examined using resistive MHD simulations. These simulations have been performed using the NIMROD code with fixed boundary flux (including NSTX poloidal coil currents) in the NSTX experimental geometry. Simulations show that an X point is formed in the injector region, followed by formation of closed flux surfaces within 0.5 ms after the driven injector voltage and injector current begin to rapidly decrease. As the injector voltage is turned off, the field lines tend to untwist in the toroidal direction and magnetic field compression exerts a radial $\mathbf{J} \times \mathbf{B}$ force and generates a bi-directional radial $E_{\text{toroidal}} \times B_{\text{poloidal}}$ pinch flow to bring oppositely directed field lines closer together to reconnect. At sufficiently low magnetic diffusivity (high Lundquist number), and with a sufficiently narrow injector flux footprint width, the oppositely directed field lines have sufficient time to reconnect (before dissipating), leading to the formation of closed flux surfaces. The reconnection process is shown to have transient Sweet-Parker characteristics. © 2013 AIP Publishing LLC. [<http://dx.doi.org/10.1063/1.4821974>]

Non-inductive current formation is a major physics objective in NSTX as an advanced Spherical Torus (ST) and in future ST-based fusion devices.¹ The ST confinement concept is projected to operate at very high values of the toroidal beta and bootstrap current fraction and is a potential candidate for a Fusion Nuclear Science Facility (FNSF).¹ However, due to the restricted space for a central solenoid in an ST, elimination of the central solenoid is likely necessary for an ST based reactor or a component test facility. This could also simplify a reactor based on the tokamak concept. Coaxial Helicity Injection (CHI) is a promising candidate for plasma start-up and may also have the potential for edge current drive during the sustained operating phase.^{2,3} Here, we numerically examine the physics of transient CHI for start-up in NSTX (for implementation of CHI on NSTX see Fig. 1 in Ref. 4). Our results reveal the fundamental mechanism for closed flux generation in transient CHI discharges. We find that it also has some universal aspects of reconnection physics. Specifically, closed flux surfaces during transient CHI could be explained through 2-D Sweet-Parker type reconnection,⁵ and 3-D non-axisymmetric modes do not appear to play a dominant role. There are similarities between the transient Sweet-Parker reconnection found here and that reported in forced-reconnection laboratory plasmas.^{6,7}

A CHI discharge is initiated by driving current along open poloidal magnetic field lines that connect the lower inner and outer divertor plates that are electrically separated from each other. In CHI terminology this region is referred to as the injector and the opposite end of the machine containing the upper divertor plates, the absorber. The initial magnetic flux connecting the lower divertor plates is referred to as the injector flux. It is produced by driving current in the lower divertor coils.

After the injector current exceeds a threshold level such that the $J_{\text{pol}} \times B_{\text{tor}}$ exceeds the field line tension of the injector flux, the injector flux gets stretched into the vessel.

Unlike *driven* CHI (edge current drive) where non-axisymmetric MHD activity is required to relax the current inward, in *transient* CHI only axisymmetric reconnection is believed to be adequate for generating a high quality closed flux start-up equilibrium. In transient CHI, on the time scales needed to fill the open flux plasma into the vessel, the injector current is rapidly reduced in magnitude. This has the effect that the injected poloidal flux is no longer being supported by the $\mathbf{J} \times \mathbf{B}$ forces and rapidly begins to pull back into the injector. Experimentally, it has been observed that if the injector flux footprints are sufficiently narrow, then during the poloidal flux decay phase, the injected poloidal flux can reconnect near the injection electrodes and result in the formation of closed flux surfaces.⁴ Formation of closed flux surfaces is essential for subsequent non-inductive current ramp-up to the levels required for sustained operation in an FNSF.¹ While some aspects of transient CHI, including scaling of CHI generated current with injector and toroidal fluxes, has been simulated using the 2-D TSC code,⁸ detailed reconnection physics has not been studied. Understanding the fundamental physics, which leads to field line reconnection, during transient CHI, is the primary purpose of this paper.

To understand the physics of reconnection and flux closure, and to more fully model the transient CHI process, we perform resistive MHD simulations of CHI for an NSTX-like discharge using the NIMROD code.⁹ Resistive MHD simulations have been used to study helicity injection physics in other configurations,^{10–12} and is well suited for studying the initial dynamic phase of a transient CHI discharge. To study the underlying physics, using the NSTX vessel geometry, we start with a simplified configuration. In these initial

^{a)}Electronic mail: ebrahimi@princeton.edu

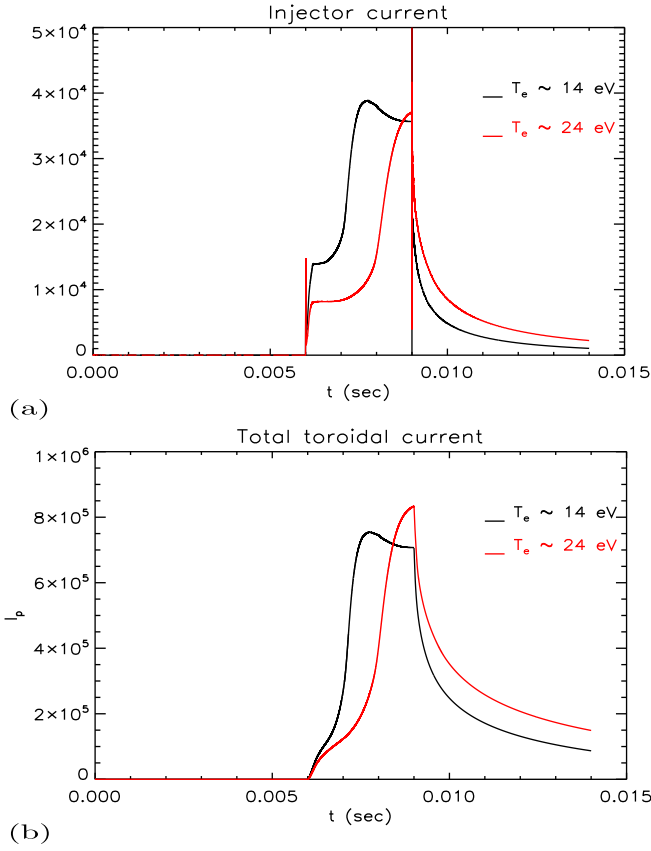


FIG. 1. Time histories of (a) injector current (RB_ϕ above the injector slot) (b) total toroidal current for simulations at $\eta = 8 \text{ m}^2/\text{s}$ ($T_e \approx 14 \text{ eV}$), and $\eta = 3.5 \text{ m}^2/\text{s}$ ($T_e \approx 24 \text{ eV}$).

simulations, we use constant poloidal field coil currents to generate the injector flux (fixed boundary flux simulations). Resistive MHD simulations with time-varying boundary conditions arising from poloidal-field coil changes in the experiment have been performed and produce closed surfaces.¹³ However, the more complete physics model therein complicates a full understanding of the reconnection and closed flux process. The present work addresses this physics using a simpler model, allowing a fuller and more detailed determination of this physics, which is important for transient CHI scaling to future devices. Under these conditions, the injector voltage is adjusted so that the $\mathbf{J} \times \mathbf{B}$ force sufficiently overcomes the field line tension¹⁴ and open field line plasma fills the vessel. Then, as in the experiment, the injector current is rapidly reduced, by turning off the applied voltage across the injector. Magnetic diffusivities similar to those in the experiment are used. However, we use an arbitrary injector flux (Ψ_{inj}) of about 70 mWb that results in a toroidal current of about 700 kA. Since the objective is to understand flux closure, the actual magnitude of plasma current which is expected to scale as Ψ_{inj} ⁸ is not important here.

The results described below provide a detailed explanation of the response of the plasma as the CHI drive is rapidly switched off, and offer insight to the experimental observations as well as the reconnection physics.

In our initial simulations, axisymmetric time-dependent resistive MHD simulations for a zero pressure model are evolved

$$\rho \left(\frac{\partial \mathbf{V}}{\partial t} + \mathbf{V} \cdot \nabla \mathbf{V} \right) = \mathbf{J} \times \mathbf{B} - \nabla \cdot \Pi, \quad (1)$$

$$\frac{\partial \mathbf{B}}{\partial t} = -\nabla \times \mathbf{E}, \quad (2)$$

$$\mathbf{E} = -\nabla \times \mathbf{B} + \eta \mu_0 \mathbf{J}, \quad (3)$$

$$\mu_0 \mathbf{J} = \nabla \times \mathbf{B}, \quad (4)$$

where η is the magnetic diffusivity. The unmagnetized part of the stress tensor Π is treated as $-\rho \nu \nabla^2 \mathbf{V}$, where ν is the viscous diffusivity. To avoid currents flowing along the top surface of the domain, a layer of large resistivity is used and the viscosity is enhanced by a factor of 30. A similar condition is imposed across the injector flux footprints and the gap in the injector region to aid numerical resolution of the boundary layer. The magnetic diffusivities used in these simulations are in the range of 3–400 m^2/s . The kinematic viscosities are chosen to give a $\text{Pm} = 7.5$ (Prandtl number = ν/η) for all the values of magnetic diffusivities used here. The viscosity is not playing a significant role in understanding the qualitative dynamics of reconnection.

A simplified waveform of injector voltage with a constant voltage ($\approx 1 \text{ kV}$) is applied at 6 ms and turned off at 9 ms. For the chosen conditions in the injector and divertor coils, this allows adequate injector current to flow along the injector flux and an open fieldline discharge fills the vessel. Current flow across the absorber gap is kept zero by setting $\Delta B_\phi = 0$ in the region between the upper divertor plates. The boundary fields and flux are kept constant ($t = 0\text{--}14 \text{ ms}$). To give converged results higher order finite elements of 45×90 fourth and fifth orders are used.

Using simulations at zero pressure, we first investigate the effect of magnetic diffusivity (or Lundquist number) on the physics of flux closure. Simulations with large magnetic diffusivity $\eta = 400 \text{ m}^2/\text{s}$ (equivalent to $T_e = 1 \text{ eV}$) show no flux closure. A small volume of closed flux forms at magnetic diffusivities of about $\eta \sim 40\text{--}20 \text{ m}^2/\text{s}$. The volume of closed flux surfaces increases as the magnetic diffusivity is reduced to $\eta \sim 8 \text{ m}^2/\text{s}$ (equivalent to $T_e = 14 \text{ eV}$). Time histories of injector current and total plasma current for two sets of simulations, $\eta \sim 8 \text{ m}^2/\text{s}$ and $\eta \sim 3.5 \text{ m}^2/\text{s}$ (equivalent to $T_e = 24 \text{ eV}$) are shown in Fig. 1. Both simulations reach similar values of injector current of about 36–37 kA at the time that the voltage is turned off. About 1 ms after the voltage is turned off, the injector currents drop sharply to about 10%–20% of their maximum values during the injection phase.

The formation of an X point and closed flux surfaces is confirmed with the field line tracing of the Poincare plots shown in Fig. 2(a). An X point starts to form at around $t = 9.005 \text{ ms}$ and *simultaneously* closed flux surfaces begin to form. The flux closure with large volume occurs around $t = 9.25 \text{ ms}$. The flux closure persists to about $t = 10 \text{ ms}$. Poincare plots of flux surfaces at $t = 9.4 \text{ ms}$ is shown in Fig. 2(a). Toroidal current in the closed flux surfaces is about 8% of the total plasma current at $t = 9.4 \text{ ms}$ (at the beginning of flux closure) and reaches a maximum of about 11% at around $t = 9.8 \text{ ms}$. Similar reconnection process and flux closure

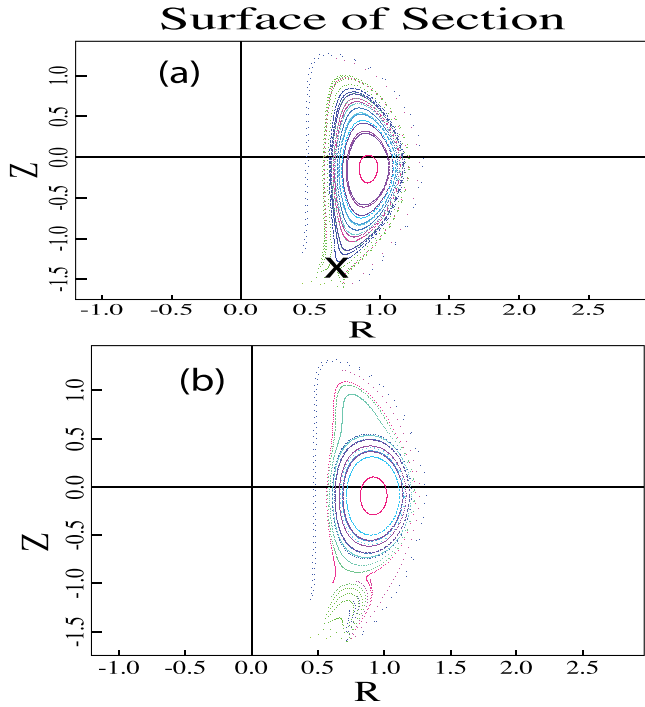


FIG. 2. Poincaré plots soon after the flux closure for the two cases (a) with $\eta = 8 \text{ m}^2/\text{s}$ at $t = 9.4 \text{ ms}$ (b) with $\eta = 3.5 \text{ m}^2/\text{s}$ at $t = 9.66 \text{ ms}$.

also occur at lower magnetic diffusivity (higher temperature). However, a larger volume of closed flux is formed at lower magnetic diffusivity $\eta \sim 3.5 \text{ m}^2/\text{s}$ (Fig. 2(b)). Flux closure with large volume starts at around $t = 9.3 \text{ ms}$ and also persists to around $t = 10 \text{ ms}$. The toroidal current in the closed volume of flux surfaces is about 13% of the total current at $t = 9.5 \text{ ms}$ and increases to about 15.5% at $t = 9.8 \text{ ms}$, which is larger than the lower temperature case.

These simulations have further elucidated the fundamental physics mechanism of flux closure and reconnection process. The formation of the X point can be explained through the Lorentz forces and flows at the reconnection site. We first examine the radial component of total Lorentz force, $(\mathbf{J} \times \mathbf{B})_r = -\nabla(B_r^2 + B_z^2 + B_\phi^2)_r/2\mu_0 + (\mathbf{B} \cdot \nabla \mathbf{B})_r/\mu_0$, which consists of the force from magnetic compression and the magnetic curvature term, (first and second terms, respectively). We should note that field consists of a fixed background field and evolving axisymmetric fields ($\mathbf{B} = \mathbf{B}_0 + \tilde{\mathbf{B}}$) during helicity injection. We calculate the quadratic terms with evolving fields, i.e., $B_0 \tilde{B}$ and \tilde{B}^2 terms, since B_0^2 terms are fixed before and after the reconnection and cannot explain the reconnection process. The poloidal curvature term also does not enter in the total force (the radial part $(B_r B_r')$, cancels out with the radial part of the compression force and the vertical Z part, $B_z dB_r/dz$ has numerically been calculated to be very small). We therefore have the two main contributions to the total force, which are $-\nabla(B_z^2 + B_\phi^2)/2\mu_0$ and $-B_\phi^2/r\mu_0$ and have been plotted before and after X point formation in Fig. 3(a). The magnetic compression force from poloidal magnetic field, $-\nabla(B_z^2)/2\mu_0$, is also calculated, but has a smaller contribution to the total force. We find that the toroidal field compression force cancels out the toroidal curvature term and results in a small radial force before the

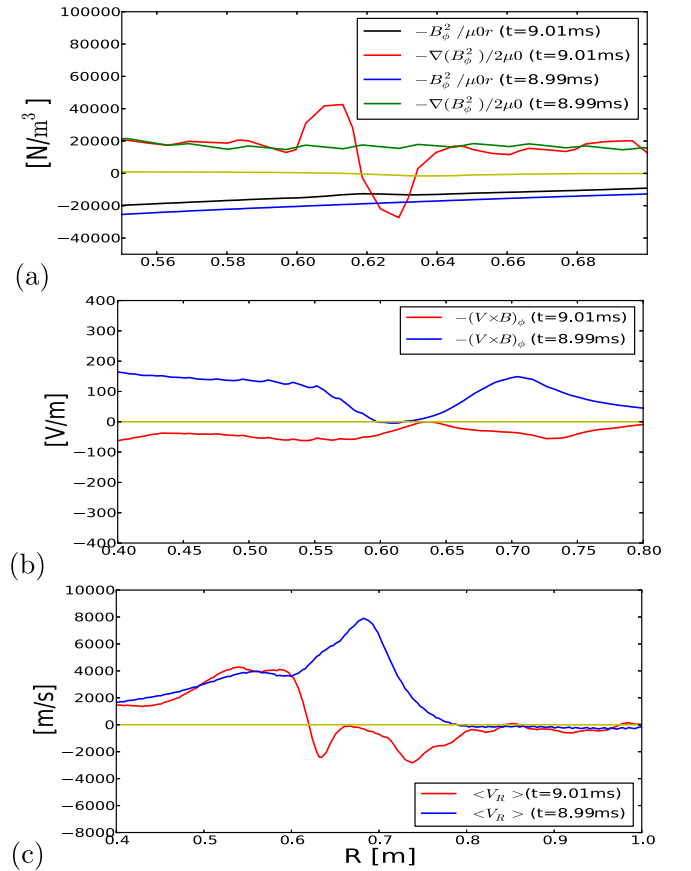


FIG. 3. Profiles of (a) $-\nabla(B_\phi^2)/2\mu_0$ and $-B_\phi^2/r\mu_0$ terms (b) induced toroidal electric field, (c) radial flows around the injector region ($z = -1.4$) before and during X point formation. All the fields are total including vacuum and evolving fields.

reconnection. However, as the injector voltage is turned off and the evolving toroidal magnetic field decreases in the injector region, the compression from the toroidal magnetic field exerts an effective bidirectional pinch force that brings the oppositely directed fields together to reconnect. It should be noted that the poloidal field compression may also contribute equally to the force when the helicity drive is reduced.

Consistent with the bidirectional pinch force, as the injector voltage is turned off, a radial pinch $\mathbf{E} \times \mathbf{B}$ flow is generated, where the electric field (loop voltage) in the toroidal direction induces the poloidal-field evolution that leads to reconnection. An induced positive loop voltage during the decay phase of CHI has also been shown in TSC simulations.⁸ Here, our simulations show that oppositely directed magnetic flux (primarily the poloidal magnetic field, B_z) around the injector region collapses together through this oppositely directed flow $V_R \approx E_\phi B_z$ and causes reconnection to occur. The radial profiles of induced toroidal electric field [$E_\phi = -(\mathbf{V} \times \mathbf{B})_\phi$] around the injection region ($z = -1.4$) before and after reconnection are shown in Fig. 3(b). This toroidal electric field that induces the evolution in poloidal flux reflects the important generation of pinch flow. The radial flow before reconnection time ($t = 8.99 \text{ ms}$) and the bidirectional pinch $\mathbf{E} \times \mathbf{B}$ flow during reconnection ($t = 9.01 \text{ ms}$) are shown in Fig. 3(c). The radial pinch flows that result in the

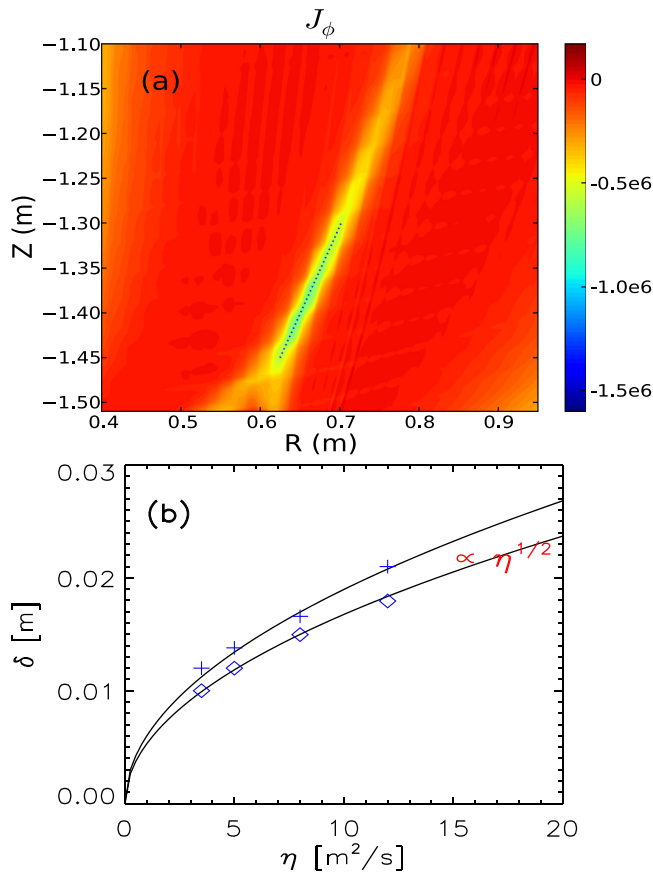


FIG. 4. (a) Elongated current sheet and (b) scaling of the current sheet layer with η during the X point formation. Diamonds and crosses obtained using a fit to a Harris type profile and half width of the vertically averaged profile, respectively.

formation of an X point at around $z = -1.35$ m causes the local poloidal flow to become very small.

To further investigate the nature of the reconnection process, we have performed a scaling of current sheet width with magnetic diffusivity. During the X point formation, local current density is further localized to form an *elongated* current sheet (Fig. 4(a)). We have calculated the width of this current sheet density around the injector region for a few values of η with the same injector current. We first have performed a coordinate transformation to coordinates aligned with the current sheet (shown with dotted black line in Fig. 4(a)) and we have confirmed that the reconnecting field (B_z) fits well with a 1-D Harris sheet type profile [$\propto \tanh(R/\delta)$].¹⁵ Using this fit, we have then calculated δ , the width of current sheet, which scales with magnetic diffusivity close to $\eta^{1/2}$. This suggests that the reconnection process during the X point formation in transient CHI may be a Sweet-Parker type reconnection. We should note that, because of the transient nature of the process, the distinction between reconnection and diffusion is lost at

higher values of η (values above $\eta_{\text{cutoff}} \approx 40 \text{ m}^2/\text{s}$ for our parameters). This emphasizes the importance of a narrow flux footprint width.

These new results from the NIMROD simulations are now able to provide a much better physical understanding of some of the experimental observations. First, we find that there are two conditions that may suppress the effective reconnection during transient CHI. If the voltage is not being rapidly reduced to zero, the injector voltage still dominates and any residual effects from the decaying poloidal flux are too small to cause reconnection. Second, if resistivity is large and the footprints are far apart, even in the presence of pinch flow, reconnection does not occur. This is because the time scales for the oppositely directed field lines to come together are longer than the poloidal flux decay time due to high resistivity. Finally, through direct numerical calculations of the radial forces, we found that as the injector voltage is turned off, a radial bi-directional pinch flow causes the field lines to reconnect.

We would like to thank A. Bhattacharjee, J. Menard, S. Kaye, and R. Kulsrud for their helpful comments. This work is supported by DOE at PU DOE-FG02-12ER55115 and CMSO, PSI Center DE-FC02-05ER54813, LLNL DE-AC52-07NA27344, and DE-FG02-99ER54519.

¹J. E. Menard, M. G. Bell, R. E. Bell, S. Bernabei, J. Bialek, T. Biewer, W. Blanchard, J. Boedo, C. E. Bush, M. D. Carter *et al.*, *Nucl. Fusion* **47**, 645 (2007).

²X. Z. Tang and A. H. Boozer, *Phys. Plasmas* **11**, 171 (2004).

³R. H. Weening, *Phys. Plasmas* **18**, 122503 (2011).

⁴R. Raman, B. A. Nelson, M. G. Bell, T. R. Jarboe, D. Mueller, T. Bigelow, B. Leblanc, R. Maqueda, J. Menard, M. Ono *et al.*, *Phys. Rev. Lett.* **97**, 175002 (2006).

⁵P. A. Sweet, in *Electromagnetic Phenomena in Cosmical Physics*, edited by B. Lehnert (IAU, 1958), Vol. 6, p. 123; E. N. Parker, *J. Geophys. Res.* **62**, 509, doi:10.1029/JZ062i004p00509 (1957).

⁶H. Ji, M. Yamada, S. Hsu, and R. Kulsrud, *Phys. Rev. Lett.* **80**, 3256 (1998).

⁷M. Yamada, H. Ji, S. Hsu, T. Carter, R. Kulsrud, and F. Trintchouk, *Phys. Plasmas* **7**, 1781 (2000).

⁸R. Raman, S. C. Jardin, J. Menard, T. R. Jarboe, M. Bell, D. Mueller, B. A. Nelson, and M. Ono, *Nucl. Fusion* **51**, 113018 (2011).

⁹C. R. Sovinec, A. H. Glasser, T. A. Gianakon, D. C. Barnes, R. A. Nebel, S. E. Kruger, D. D. Schnack, S. J. Plimpton, A. Tarditi, M. Chu *et al.*, *J. Comput. Phys.* **195**, 355 (2004).

¹⁰C. R. Sovinec and S. C. Prager, *Phys. Plasmas* **3**, 1038 (1996).

¹¹E. B. Hooper, B. I. Cohen, H. S. McLean, R. D. Wood, C. A. Romero-Talamás, and C. R. Sovinec, *Phys. Plasmas* **15**, 032502 (2008).

¹²R. A. Bayliss, C. R. Sovinec, and A. J. Redd, *Phys. Plasmas* **18**, 094502 (2011).

¹³E. B. Hooper, C. R. Sovinec, R. Raman, F. Ebrahimi, and J. E. Menard, "Resistive MHD simulation of helicity-injected startup plasmas in NSTX," *Phys. Plasmas* (to be published).

¹⁴T. R. Jarboe, *Fusion Technol.* **15**, 7 (1989).

¹⁵E. G. Harris, *Nuovo Cimento* **23**, 115 (1962).